

Numerical characterizations of a piezoelectric micromotor using topology optimization design

M. Sadeghbeigi Olyaie* and M.R. Razfar

Mechanical Engineering Department, Amirkabir University of Technology, Tehran, Iran

(Received March 6, 2012, Revised May 28, 2012, Accepted August 17, 2012)

Abstract. This paper presents the optimum load-speed diagram evaluation for a linear micromotor, including multitude cantilever piezoelectric bimorphs, briefly. Each microbeam in the mechanism can be actuated in both axial and flexural modes simultaneously. For this design, we consider quasi-static and linear conditions, and a relatively new numerical method called the smoothed finite element method (S-FEM) is introduced here. For this purpose, after finding an optimum volume fraction for piezoelectric layers through a standard numerical method such as quadratic finite element method, the relevant load-speed curves of the optimized micromotor are examined and compared by deterministic topology optimization (DTO) design. In this regard, to avoid the overly stiff behavior in FEM modeling, a numerical method known as the cell-based smoothed finite element method (CS-FEM, as a branch of S-FEM) is applied for our DTO problem. The topology optimization procedure to find the optimal design is implemented using a solid isotropic material with a penalization (SIMP) approximation and a method of moving asymptotes (MMA) optimizer. Because of the higher efficiency and accuracy of S-FEMs with respect to standard FEMs, the main micromotor characteristics of our final DTO design using a softer CS-FEM are substantially improved.

Keywords: topology optimization; cell based smoothed finite element method; piezoelectric micromotor

1. Introduction

Because of various advanced applications of actuators in industry, especially piezoelectric actuators, the dimensions of linear actuators are gradually being reduced to even beyond the range of microelectromechanical systems (MEMS) devices (Ueha and Tomikawa 1993).

Currently, the most common and efficient strategy for design of these structures is the deterministic optimization or DTO model (Arora 2004, Bendsoe and Sigmund 2003, Bendsoe and Kikuchi 1988). Topology optimization using a solid isotropic material with a penalization (SIMP) approximation is the simplest and most popular technique (Rozvany *et al.* 1992). Design variables in the optimization process can also be updated through some numerical algorithms such as a powerful optimizer tool known as the method of moving asymptotes (MMA) proposed by Svanberg (1987).

A simple numerical optimization procedure is shown in Fig. 1. For this problem, after initial data setting up and finding optimum piezoelectric volume fraction, design variable updating is

*Corresponding author, Ph.D, E-mail: m.sadeghbeigi@aut.ac.ir

started. Based on this figure, the major task under the updating loop for the optimization (or topology optimization) procedure needs to be handled by a stable and efficient numerical method such as the finite element method (FEM). For piezoelectric analyses, to increase stress accuracy of the computations and to decrease element distortions sensitivity due to the overly stiff behavior of the standard FEMs models, approaches such as the piezoelectric finite element with drilling degrees of freedom (Long *et al.* 2006), hybrid formulations (Sze *et al.* 2004), and meshless methods such as the meshless point collocation method (PCM) and radial point interpolation method (RPIM) have been developed (Ohs and Aluru 2001, Liu *et al.* 2003). Recently, the smoothed finite element method (S-FEM) has been proposed by Nguyen *et al.* (2009) to overcome these numerical drawbacks.

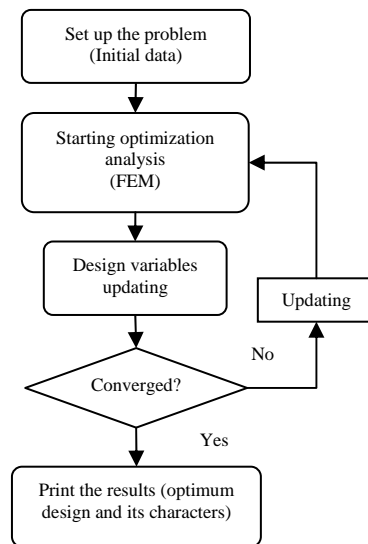


Fig. 1 Typical flowchart for a numerical optimization

This method combines parts of the standard FEM and meshless techniques (Chen *et al.* 2001), was developed by Liu *et al.* (2007). This method states that numerical analyses of static and dynamic problems through S-FEMs are always more stable than standard FEMs, due to softening effects provided by smoothing operations in the S-FEM (Bordas *et al.* 2010). As such, the S-FEM numerical results are often found to be even more accurate than those of standard FEMs with the same degrees of freedom, (Liu *et al.* 2009, Liu and Nguyen 2010, Liu *et al.* 2007, Nguyen *et al.* 2009, Liu *et al.* 2010). Based on Fig. 1, after converging of the optimization loop, the final optimum design will be achieved.

To date, most investigations on piezoelectric topology optimizations, such as that by Silva and Kikuchi (1999), Silva (2003), Begg and Liu (2000), Carbonari *et al.* (2006), Carbonari *et al.* (2005), Kogl and Silva (2005), Kang and Wang (2010), Donoso and Sigmund (2009), and Kim *et al.* (2010) have focused on optimizations through standard FEM algorithms. Because of the important role of finite element models on final optimization results, the topology optimization of the prescribed piezoelectric micromotor, proposed by Friend *et al.* (2004) using the softer CS-FEM

has been evaluated by Sadeghbeigi Olyaie *et al.* (2011) with just considering a constant volume fraction for piezoelectric materials (equal to 50%). However for more efficiency, before applying topology optimization algorithm, it is really necessary to compute the piezoelectric optimum volume fraction (weight) as an input data for optimization process. Then, the most critical specifications of the optimized mechanism, including load-speed diagram, weight and dimensions, are characterized. Therefore, these necessary optimum data for the mentioned piezoelectric micromotor will be further discussed in this paper.

The remainder of this paper is organized as follows. The design concept of an actuator will be discussed in section 2. The S-FEM and cell-based smoothed finite element method are then introduced in section 3. Next, the framework of topology optimization will be explained in section 4, and in section 5 the problem algorithm will be explained. In section 6, an optimum piezoelectric volume fraction using Q4-FEM for this micromotor will be evaluated, and the DTO numerical results of this actuator analysis based on Q4-FEM, T3-FEM, and CS-FEM besides numerical characterizations of the optimal micromotor will be compared, examined, and discussed in detail. Finally, conclusions of this research will be briefly explained.

2. Concept design of the used piezoelectric micromotor

The operating concept of the linear micromotor used in this study is based on the axial and transverse motions of bimorph piezoelectric cantilevers as shown schematically in Fig. 2 (Friend *et al.* 2004). Detailed information about each bimorph can be seen in Fig. 3; in the figure, each beam includes an elastic material interface with low magnetic permeability (such as phosphor bronze), two piezoelectric layers with the same polarization direction, and finally some relevant electrodes for applying electric fields. By applying an electric field simultaneously on all four electrodes according to Fig. 3(a), an elliptical motion will be generated. By creating a suitable phase shifting on the piezoelectric sequentially bimorphs, and then by generating a preload force on the system, a linear motion will be produced (Fig. 2 (Sadeghbeigi Olyaie *et al.* 2011)). Recently, a Swedish company (PiezoMotor AB) has been commercially manufacturing this type of linear motor.

3. Cell-based smoothed finite element method formulations for piezoelectric problems

For linear conditions, the matrix form of the constitutive equation for a piezoelectric structure can be written as

$$\begin{Bmatrix} \mathbf{T} \\ \mathbf{D} \end{Bmatrix} = \begin{bmatrix} c_E & -e^T \\ e & \varepsilon_s \end{bmatrix} \begin{Bmatrix} \mathbf{S} \\ \mathbf{E} \end{Bmatrix}. \quad (1)$$

In this equation, \mathbf{T} and \mathbf{S} denote the stress and strain vectors, \mathbf{D} and \mathbf{E} are the electric displacement and electric field vectors, c_E , e , and ε_s are the elastic material property matrix at a constant electric field, and piezoelectric and dielectric matrices at a constant mechanical strain, respectively.

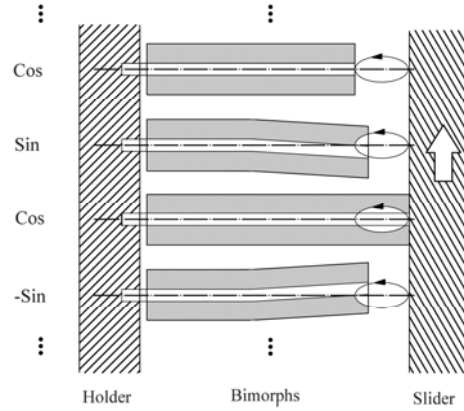


Fig. 2 Operational mechanism of the considered piezoelectric linear micromotor (Friend *et al.* 2004)

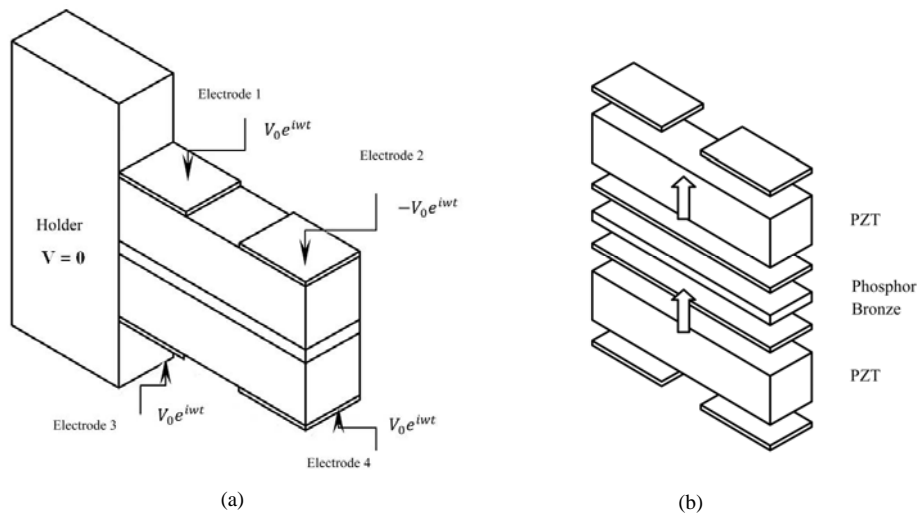


Fig. 3 Bimorph beam used to construct the linear micromotor: (a) assembled and (b) its components (Friend *et al.* 2004)

For a standard FEM analysis of piezoelectric materials, the compatibility relations between the strain-displacement, electric field-potential, displacement and electric potential can be written as (Nguyen *et al.* 2009)

$$\mathbf{S} = \nabla \mathbf{u} ; \quad \nabla = \begin{bmatrix} \frac{\partial}{\partial x} & 0 & \frac{\partial}{\partial y} \\ 0 & \frac{\partial}{\partial y} & \frac{\partial}{\partial x} \end{bmatrix}^T \quad (2)$$

$$\mathbf{E} = -\text{grad}(\phi) \quad (3)$$

$$\mathbf{u}(\mathbf{x}) = \sum_{I=1}^n \begin{bmatrix} \mathbf{N}_I(\mathbf{x}) & 0 \\ 0 & \mathbf{N}_I(\mathbf{x}) \end{bmatrix} \mathbf{d}_I ; \phi(\mathbf{x}) = \sum_{I=1}^n \mathbf{N}_I(\mathbf{x}) \phi_I \quad (4)$$

where \mathbf{u} is the mechanical displacement, ϕ relates to the electric potential vector, n, \mathbf{d}_I, ϕ_I , and $\mathbf{N}_I(\mathbf{x})$ are the total number of nodes in the design domain, nodal displacement vector, nodal electric potential vector, and (linear) shape function, respectively.

When the S-FEM is used, especially for this study, because of the multi-material and multi-layer conditions cell-based S-FEM (CS-FEM) is preferred (Liu and Nguyen 2010, Liu *et al.* 2010).

For a quadratic CS-FEM, Fig. 4 schematically presents the smoothing domains associated with the different number of cells (nSC) (Liu *et al.* 2010). For this type of analysis, the smoothed strains ($\tilde{\mathbf{S}}$) and smoothed electric fields ($\tilde{\mathbf{E}}$) for a piezoelectric structure can be written as (Liu *et al.* 2010)

$$\tilde{\mathbf{S}} = \frac{1}{A^{(c)}} \int_{\Gamma^{(c)}} \mathbf{n}_u^{(c)} \mathbf{u}(\mathbf{x}) d\Gamma = \sum_{I \in N_n} \tilde{\mathbf{B}}_{uI}(\mathbf{x}_c) \mathbf{d}_I \quad (5)$$

$$\tilde{\mathbf{E}} = -\frac{1}{A^{(c)}} \int_{\Gamma^{(c)}} \mathbf{n}_\phi^{(c)} \phi(\mathbf{x}) d\Gamma = - \sum_{I \in N_n} \tilde{\mathbf{B}}_{\phi I}(\mathbf{x}_c) \phi_I \quad (6)$$

where $\Gamma^{(c)}$ is the boundary of the smoothing domain ($\Omega^{(c)}$) associated with a cell (c), N_n is the number of element nodes, $\tilde{\mathbf{B}}_{uI}(\mathbf{x}_c)$ and $\tilde{\mathbf{B}}_{\phi I}(\mathbf{x}_c)$ are the smoothed strain and smoothed electric field matrixes on the domain ($\Omega^{(c)}$), respectively, and $\mathbf{n}_u^{(c)}$ and $\mathbf{n}_\phi^{(c)}$ are the normal outward vectors on the boundary ($\Gamma^{(c)}$), such that

$$\mathbf{n}_u^{(c)} = \begin{bmatrix} \mathbf{n}_x^{(c)} & 0 \\ 0 & \mathbf{n}_y^{(c)} \\ \mathbf{n}_y^{(c)} & \mathbf{n}_x^{(c)} \end{bmatrix} ; \mathbf{n}_\phi^{(c)} = \begin{bmatrix} \mathbf{n}_x^{(c)} & \mathbf{n}_y^{(c)} \end{bmatrix}^T. \quad (7)$$

Note that the values of $\tilde{\mathbf{B}}_{uI}(\mathbf{x}_c)$ and $\tilde{\mathbf{B}}_{\phi I}(\mathbf{x}_c)$ are

$$\tilde{\mathbf{B}}_{uI}(\mathbf{x}_c) = \frac{1}{A^{(c)}} \sum_{b=1}^{nb} \begin{bmatrix} \mathbf{N}_I(\mathbf{x}_b^g) \mathbf{n}_x^{(c)}(\mathbf{x}_b^g) & 0 \\ 0 & \mathbf{N}_I(\mathbf{x}_b^g) \mathbf{n}_y^{(c)}(\mathbf{x}_b^g) \\ \mathbf{N}_I(\mathbf{x}_b^g) \mathbf{n}_y^{(c)}(\mathbf{x}_b^g) & \mathbf{N}_I(\mathbf{x}_b^g) \mathbf{n}_x^{(c)}(\mathbf{x}_b^g) \end{bmatrix} l_b^{(c)} \quad (8)$$

$$\tilde{\mathbf{B}}_{\phi I}(\mathbf{x}_c) = \frac{1}{A^{(c)}} \sum_{b=1}^{nb} \begin{bmatrix} \mathbf{N}_I(\mathbf{x}_b^g) \mathbf{n}_x^{(c)}(\mathbf{x}_b^g) \\ \mathbf{N}_I(\mathbf{x}_b^g) \mathbf{n}_y^{(c)}(\mathbf{x}_b^g) \end{bmatrix} l_b^{(c)}. \quad (9)$$

Similar to the standard FEM by applying Hamilton's principle (Benjeddou 2000, Allik and Hughes 1970) the general S-FEM discretized matrix form in a smoothing space for a time-harmonic excitation problem will be changed to (Jensen 2009)

$$\tilde{\mathbf{M}}(\rho) \ddot{\mathbf{d}} + \tilde{\mathbf{C}}(\rho) \dot{\mathbf{d}} + \tilde{\mathbf{K}}(\rho) \mathbf{d} = \mathbf{f}(\rho) e^{i\omega t} \quad (10)$$

In this equation, $\hat{\mathbf{d}}$, $\mathbf{f}(\rho)$, ω , and i are the transformed shapes of instantaneous displacement, the magnitude of the applied load vector, the rotational frequency of the applied load, and the imaginary number in complex variables, respectively. With a proportional damping assumption, the smoothing stiffness matrix ($\tilde{\mathbf{K}}$) smoothing mass matrix ($\tilde{\mathbf{M}}$) and smoothing damping matrix ($\tilde{\mathbf{C}}$) will then become

$$\tilde{\mathbf{K}} = \begin{bmatrix} \tilde{\mathbf{k}}_{uu} & \tilde{\mathbf{k}}_{u\phi} \\ \tilde{\mathbf{k}}_{u\phi} & \tilde{\mathbf{k}}_{\phi\phi} \end{bmatrix}; \tilde{\mathbf{M}} = \begin{bmatrix} \mathbf{m} & 0 \\ 0 & 0 \end{bmatrix}; \tilde{\mathbf{C}} = \alpha \tilde{\mathbf{M}} + \beta \tilde{\mathbf{K}} \quad (11)$$

where α and β are the constant prescribed damping coefficients. The components of the smoothed stiffness matrix for each element domain and the mass matrix can be calculated as follows (Dai *et al.* 2007)

$$\tilde{\mathbf{K}}_{e(uu)} = \sum_c^{nSC} (\tilde{\mathbf{B}}_u^{(c)})^T c_E \tilde{\mathbf{B}}_u^{(c)} A^{(c)} \quad (12)$$

$$\tilde{\mathbf{K}}_{e(u\phi)} = \sum_c^{nSC} (\tilde{\mathbf{B}}_u^{(c)})^T e^T \tilde{\mathbf{B}}_\phi^{(c)} A^{(c)} \quad (13)$$

$$\tilde{\mathbf{K}}_{e(\phi\phi)} = - \sum_c^{nSC} (\tilde{\mathbf{B}}_\phi^{(c)})^T \varepsilon_s \tilde{\mathbf{B}}_\phi^{(c)} A^{(c)} \quad (14)$$

$$\mathbf{m} = \int_{\Omega} \rho \mathbf{N}_I^T \mathbf{N}_I d\Omega. \quad (15)$$

For topology optimization applications, all the design parameters in Eq. (10) are functions of density of each element (ρ) as the design variable.

Note that the steady state solution of Eq. (10) is

$$\hat{\mathbf{d}}(t) = \hat{\mathbf{u}}(\rho) e^{i\omega t} \quad (16)$$

where $\hat{\mathbf{u}}(\rho)$ is the magnitude of the displacement vector in complex form. By this assumption, Eq. (10) yields

$$\tilde{\mathbf{G}}(\rho, w)\hat{\mathbf{u}} = \mathbf{f}(\rho) \quad (17)$$

where $(\tilde{\mathbf{G}}(\rho, w))$ is a dynamic stiffness matrix equal to

$$\tilde{\mathbf{G}}(\rho, w) = -w^2\tilde{\mathbf{M}}(\rho) + iw\tilde{\mathbf{C}}(\rho) + \tilde{\mathbf{K}}(\rho). \quad (18)$$

As can be seen in the above equations, only the calculation of the stiffness matrix in the CS-FEM method is different from the standard FEM computations.

The solution of the CS-FEM with $nSC = 1$ is equal to the standard FEM solution using reduced integration points (upper bound solution with flexible stiffness). If the number of smoothed domains for each element approaches infinity, the solution will approach the full integration standard FEM solution with (2×2) Gauss integration (lower bound solution with stiff stiffness). Finally, if $1 < nSC < \infty$ the CS-FEM model is always softer than the FEM using the same set of elements, and the CS-FEM solution (in strain energy) falls between the upper-bound and lower-bound FEM solutions of the force driving problems (Liu *et al.* 2007). Since the displacement conformity in this method is only valid along the edges of each cell, the computed stiffness matrices and displacements obtained through this method will be more flexible and more accurate than the standard FEM values, respectively (Chen *et al.* 2001, Liu *et al.* 2007, Liu *et al.* 2007).

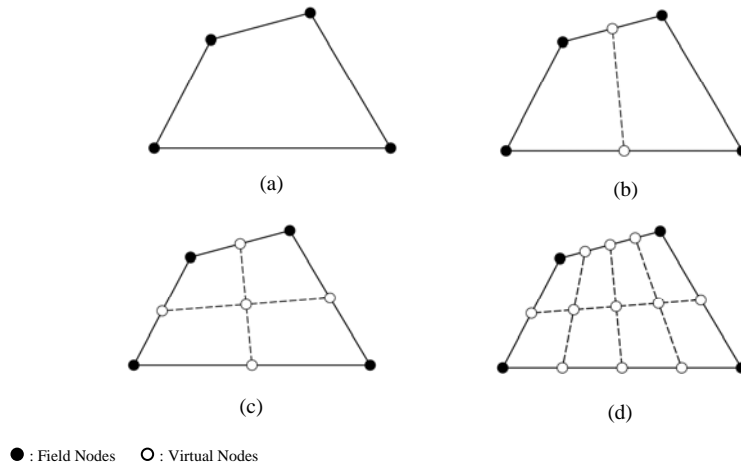


Fig. 4 Smoothing domain (SD) concepts for the CS-FEM: (a) 1 SD, (b) 2 SDs, (c) 4 SDs and (d) 8 SDs (Liu *et al.* 2010)

4. Topology optimization

This technique determines the optimum material distribution required for a system to optimize an objective function, such as velocity, with respect to some defined constraints.

The general form of a DTO problem is

$$DTO: \begin{cases} \text{Optimize : an objective function} \\ \text{Constraints : } \begin{cases} \text{Equilibrium equations} \\ \text{Volume, cost or certainty constraints} \end{cases} \end{cases} \quad (19)$$

Numerical approaches such as homogenization (Bendsoe and Kikuchi 1988) and SIMP techniques (Rozvany *et al.* 1992, Bendsoe 1989) are commonly used to determine topology optimization designs. The homogenization model uses microscopic material distribution to find the optimum solution, whereas the SIMP method employs the pseudo density of each element as a design variable. Since the SIMP method implementation is relatively simpler and is more efficient than the homogenization model, this algorithm is usually preferred.

The SIMP technique can be successfully applied for multi-constraints, multi-materials, and multi- physics conditions. Through this method, the intermediate densities of each element (pseudo density (ρ_e)) are penalized to distinctive values near 0 (void) or 1 (solid) (Bendsoe and Sigmund 2003).

Through the extended SIMP technique for piezoelectric structures called piezoelectric material with penalization and polarization (PEMAP-P) model, mechanical (c_E), electromechanical (e), and dielectric (ε_s) properties of these materials are interpolated (Kim *et al.* 2010) as

$$c_E = \rho_e^{nc} c_E^0 ; 0 < \rho_{min} \leq \rho_e \leq 1 \quad (20)$$

$$e = \rho_e^{ne} e^0 ; 0 < \rho_{min} \leq \rho_e \leq 1 \quad (21)$$

$$\varepsilon_s = \rho_e^{n\varepsilon} \varepsilon_s^0 ; 0 < \rho_{min} \leq \rho_e \leq 1 \quad (22)$$

where the exponents nc , ne , and $n\varepsilon$ are the material density penalization factors, and c_E^0 , e^0 , and ε_s^0 represent the nominal material matrices for the solid material case ($\rho_e = 1$). The minimum density value ($\rho_{min} = 0.01$) is mentioned here in order to avoid singularity of the stiffness matrix during the FEM solution.

Finding appropriate penalization powers is usually based on a numerical trial and error process (Bendsoe and Sigmund 1999).

4.1 Sensitivity analysis

During the design variable updating process (such as the MMA optimizer), calculation of the objective function (*Object Fun*) and related constraints differentiations with respect to design variables (ρ_e) is necessary. Here, this sensitivity analysis is conducted via an efficient method called the adjoint sensitivity analysis (Choi and Kim 2005).

For a dynamic system, an objective function can be defined using a real function (*Object Fun*₀) as (Jensen 2009)

$$Object\ Fun = Object\ Fun_0(\rho, \hat{u}_r, \hat{u}_i) \quad (23)$$

where \hat{u}_r and \hat{u}_i are the real part and imaginary parts of the displacement vector, respectively. By introducing the Lagrangian multiplier (λ), the adjoint form of this function becomes

$$Object\ Fun = Object\ Fun_0(\rho, \hat{u}_r, \hat{u}_i) + \lambda^T (\tilde{G}\hat{u} - f) + \overline{\lambda}^T (\overline{\tilde{G}}\overline{\hat{u}} - \overline{f}) \quad (24)$$

where the over bar items in Eq. (24) denote the complex conjugates.

Based on Jensen's note (2009), the final sensitivity expression then is

$$\frac{d(Object\ Fun)}{d\rho_e} = \frac{\partial(Object\ Fun_0)}{\partial\rho_e} + 2Real\left[\lambda^T\left(\frac{\partial\tilde{G}}{\partial\rho_e}\hat{u} - \frac{\partial f}{\partial\rho_e}\right)\right] \quad (25)$$

where (λ) is the solution to (Sadeghbeigi Olyaie *et al.* 2011)

$$\tilde{G}\lambda = -\frac{1}{2}\left[\frac{\partial(Object\ Fun_0)}{\partial\hat{u}_r} - i\frac{\partial(Object\ Fun_0)}{\partial\hat{u}_i}\right]^T \quad (26)$$

4.1.1 Mesh independent filtering

To overcome some numerical problems such as checkerboard regions, mesh dependency and local minima results during optimization process, sensitivity analysis filtering scheme proposed by Sigmund (1994, 1997) has been used in this work. Based on this approach, instead of using real sensitivities (e.g., Eq. (25)), the filtered objective function sensitivity is used for topology optimization computation as

$$\frac{d(\hat{Object\ Fun})}{d\rho_e} = \frac{1}{\rho_e \sum_{i=1}^{N_e} H_i} \sum_{i=1}^{N_e} \left[H_i \rho_i \frac{\partial(Object\ Fun)}{\partial\rho_i} \right] \quad (27)$$

where N_e is number of elements in design domain and H_i is the convolution operator which can be defined as

$$H_i = r - dist(e, i) \ , \ \{i \in N_e / dist(e, i) \leq r\} \quad e = 1, \dots, N_e \quad (28)$$

In this equation operator $dist(e, i)$ is defined as the distance between the center of considered element (e) and the center of element i . By choosing an appropriate filter size (r), many of the mentioned numerical problems can be removed.

5. Problem algorithm

The applied topology optimization algorithm for this study can be summarized in Fig. 5.

6. Numerical results and discussions

Numerical topology optimization results (for various numerical methods) with some of the final optimized characterizations for the prescribed mechanism (according to Figs. 2 and 3) will be examined, compared and discussed here. All computations were conducted on a PC using an *Intel® Core(TM) 2 Quad, Q9550@2.83 GHZ CPU, and 4GB RAM*.

6.1 Numerical results

6.1.1 Problem definition

The final goal of this study is to find some optimal specifications such as load-speed curve required for a linear micromotor (shown in Fig. 2) to reach the maximum linear velocity. To that end, a set of proper objective function and constraints need to be defined.

The final objective function (the end point velocity of each beam) for a constant excitation frequency can be defined to maximize the resultant end-point displacement of each microbeam (point (A) in Fig. 6 (b)). The matrix form of the objective function can thus be written as

$$Object\ Fun_0 = \hat{u}^T L \bar{\hat{u}} \quad (29)$$

where L is a diagonal matrix independent from the design variable whose non-zero diagonal entries are proportional to the position of point (A) in Fig. 6(b).

The configuration (including materials and polarization direction), design domain, and dimension of each beam are shown in Figs. 6(a), 6(b), and 7. The thickness of each beam is 1 (mm), applied voltage is 100 (volts) ($V_0 = 100(v)$), and the excitation frequency ω is 1 Hz.

The setting of this optimization problem can be summarized as follows

$$\left\{ \begin{array}{l} \text{Objective function: } -\hat{u}^T L \bar{\hat{u}} \\ \text{Design variable: } \rho_e \end{array} \right\}; \text{ Subject to: } \left\{ \begin{array}{l} \text{Equilibrium equations} \\ \sum_{e=1}^{num} Vol_e(\rho_e) \leq volfrac \\ Vol_0 \\ 0 < \rho_{min} \leq \rho_e \leq 1 \end{array} \right. \quad (30)$$

where Vol_0 , Vol_e , num and $volfrac$ are the volume of the design domain corresponding to $\rho_e = 1$, volume of each element, number of elements in the design domain, and the volume fraction ratio, respectively.

Based on the mentioned algorithm, first an optimum piezoelectric volume fraction (*volfrac*) by a standard FEM is computed, then the DTO analysis will be conducted by comparing various numerical methods.

This problem is analyzed using the following assumptions and parameters:

- The problem condition is linear and quasi-static.
- The thickness of each electrode is very small in comparison to dimensions of the other parts.
- A mesh of 100×10 elements is used.
- The radius of filter used in sensitivity filtering operation is $r = 1.7 \text{ mm}$.
- Material properties of the PZT are obtained from reference (Nguyen *et al.* 2009).

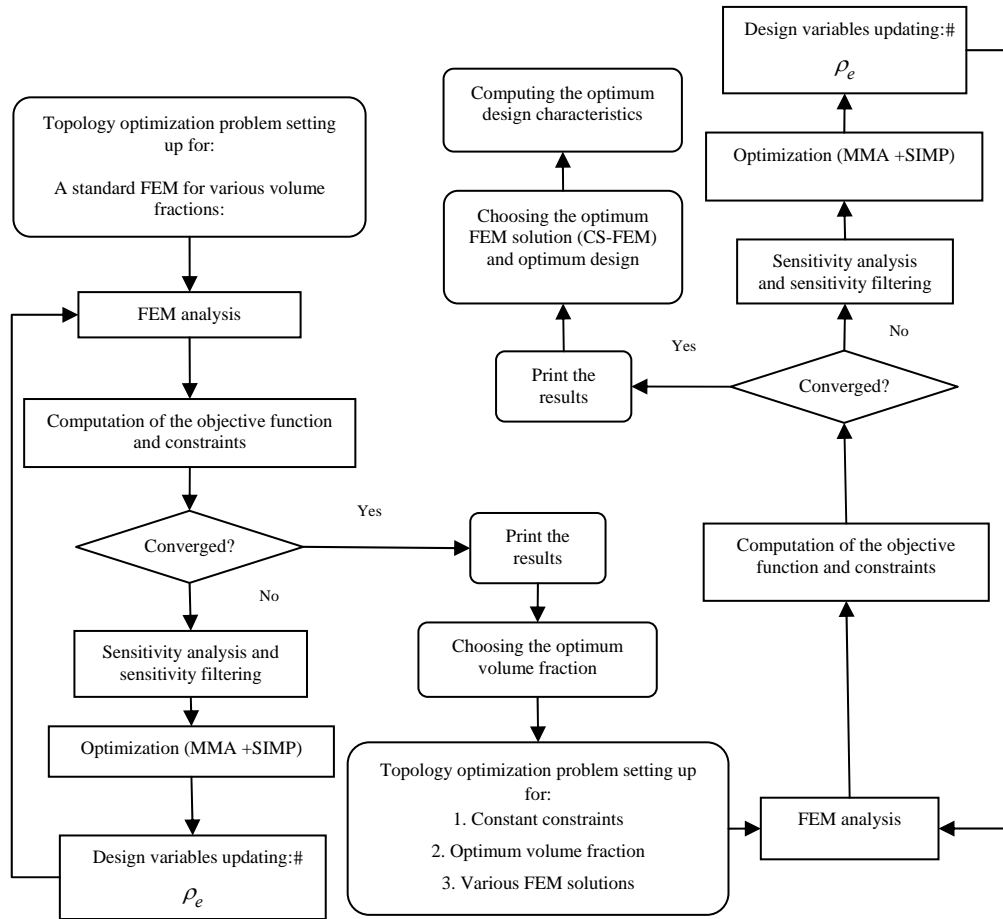


Fig. 5 General applied DTO flow chart

6.1.2 Optimum piezoelectric volume fraction

The first step in topology optimization design for this study is finding an optimum piezoelectric volume fraction in design domain. For this purpose, the maximum velocities of the prescribed mechanism for 50%, 65%, 70%, 75%, 80% and 100% of piezoelectric volume fractions are compared and evaluated.

Topology optimization results of the proposed micromotor for various piezoelectric volume fractions (50%, 65%, 70%, 75%, 80% and 100%) using a standard FEM (Q4-FEM) will be calculated here.

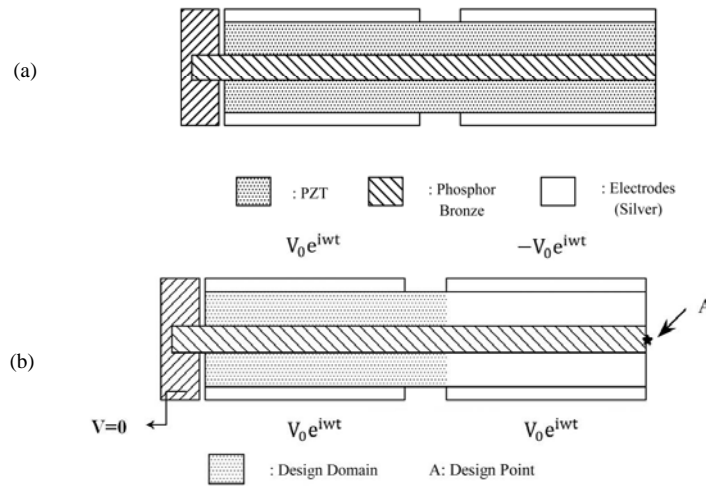


Fig. 6 Definition of the problem: (a) general configuration and (b) design domain

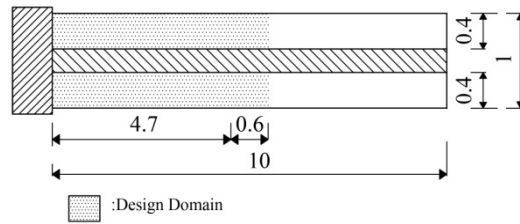


Fig. 7 Dimension of the optimization problem (based on mm)

The sensitivity analysis of the required objective function (Eq. (29)) is calculated via the adjoint variable method using Eqs.(25) and (26) as

$$\frac{d(-\hat{u}^T L \bar{\hat{u}})}{d\rho_e} = -2\text{Real}(\lambda^T \frac{\partial \tilde{G}}{\partial \rho_e} \hat{u}) \quad (31)$$

and

$$\tilde{\mathbf{G}}\boldsymbol{\lambda} = \mathbf{L}^T \bar{\mathbf{u}} \quad . \quad (32)$$

End point velocity of each beam variation respect to various piezoelectric volume fractions is graphically shown in Fig. 8. By comparing these results, it can be concluded that 70% of the piezoelectric material in design domain (Fig. 7) is the optimum volume fraction amount (*volfrac*) for Eq. (30).

6.1.3 Topology optimization designs with 70% volume fraction

The topology optimization results obtained with 70% volume fraction are summarized in table 1. These topology optimization configurations are found using different approaches, as shown in Figs. 9(a) to (e).

6.1.4 Reanalysis

Since topology optimization designs even after applying sensitivity analysis filtering procedure (according to Eq.(27)) usually include gray zones (as can be observed in Fig. 9), these structures are not generally suitable for manufacturing. To improve this defect, a reanalysis process is executed at the end of the optimization procedure (Bendsoe and Sigmund 2003). By applying this technique, the design variables (e.g., the pseudo density of each element) that are less than a threshold factor will be removed and the larger values will be approximated as the solid state condition ($\rho_e = 1$).

Based on this procedure, our final topology optimization results in comparison with initial optimization data are listed in Table 2, where the threshold factor is 0.6.

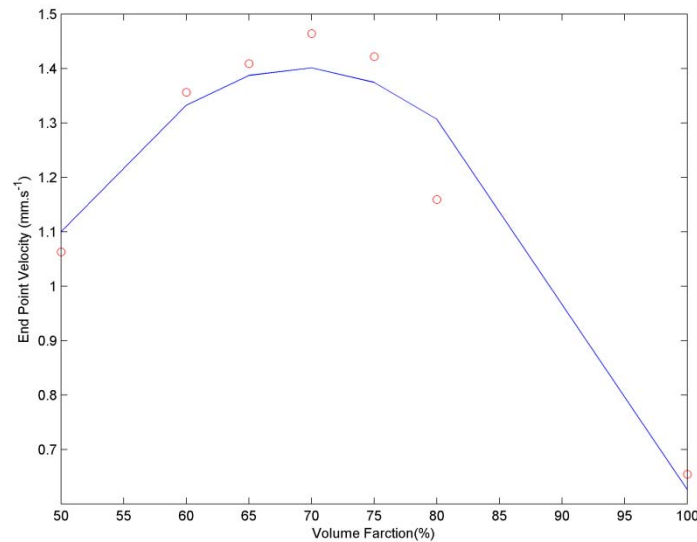


Fig. 8 Changes of piezoelectric micromotor velocity respect to design domain piezoelectric volume fraction

6.2 Discussions

It has been shown that the optimum piezoelectric volume fraction is not exactly zero or one hundred percent (70% for this problem). This result arises from the interaction between mechanical and electrical properties of piezoelectric materials. This important property is expressed as a parameter called electromechanical coupling coefficient (Chang *et al.* 1995). This factor reflects the ratio of mechanical deformation energy to applied electric potential energy. So, for this study, 70% piezoelectric volume fraction can produce maximum linear velocity.

This was also observed in the final results: when the number of smoothing domains was increased (from 2 to 8), the optimized velocity approached the Q4-FEM results. This observation provides, in a way, a validation of the CS-FEM for determining topology optimization designs when many smoothing domains are used (Liu *et al.* 2007, Liu and Nguyen 2010, Liu *et al.* 2007).

Because a smoothed strain is used inside each smoothing domain in the CS-FEM, by increasing the number of smoothing domains the final topology optimized results will have fewer checkerboard or gray regions than even the designs obtained by standard FEMs (Huang and Xie 2010). Indeed, as can be observed from the obtained results (Table 2), after the reanalysis process the optimized velocity for CS-FEM ($nSD=2$) is less than the velocity from CS-FEM ($nSD=4$).

In our study, because the final reanalysis optimal objective function (linear velocity) obtained through CS-FEM ($nSD=4$) has a higher value than the other designs (e.g., more than about 18% with respect to the Q4-FEM result), we suggest that CS-FEM ($nSD=4$) with 70% of piezoelectric material leads to the optimal design.

Table 1 Comparison of our topology optimization designs with 70% volume fraction











FEM Analysis	Initial Instantaneous Velocity (mms^{-1})	Optimized Instantaneous Velocity (mms^{-1})	Number of Iterations	Total CPU Time (min)
Q4-FEM	0.149	1.464	293	88.8
T3-FEM	0.128	0.908	455	110.0
CS-FEM ($nSD=2$)	0.166	1.971	325	91.8
CS_FEM ($nSD=4$)	0.155	1.587	318	103.7
CS_FEM ($nSD=8$)	0.152	1.580	296	116.9

6.3 Optimal numerical characterizations

According to the proposed optimal actuator chosen in discussions section, the final main specifications of this design including configuration of each microbeam in design domain (based on Fig. 6 definition), approximate weight, and velocity of micromotor for free condition in comparison with original mechanism can be summarized in table 3.

The final acquired optimum velocity mentioned in table 3 is based on free load condition, so for real solution the speed variation via applied external load should be calculated. This curve can be obtained by solving general FEM equation in Eq.(17). This result has been shown in Fig. 10. This figure emphasizes that 50(gr) is approximately the linear motor breaking load.

Table 2 Comparison of our final reanalysis designs (Threshold factor: 0.6)

FEM analysis	Initial optimized velocity (mms^{-1})	Reanalysis optimized velocity (mms^{-1})	Reanalysis volume ratio (%)	Reanalysis configuration	
Q4-FEM	1.464	0.816	0.666		
T3-FEM	0.908	0.643	0.666		
CS-FEM ($nSD=2$)	1.971	0.769	0.664		
CS-FEM ($nSD=4$)	1.587	0.962	0.668		
CS-FEM ($nSD=8$)	1.580	0.855	0.673		

7. Conclusions

Piezoelectric microactuators are extensively being used in industrial and medical science technologies. However, to attain even higher operational and economic efficiency, the optimum design of these structures is required.

The topology optimization of a prescribed linear piezoelectric micromotor needed to reach maximum velocity by satisfying the optimum volume (weight) fraction and required equilibrium equations has been evaluated in this research. The optimal volume fraction was found by comparing the topology optimization results of various volume fraction designs using Q4-FEM. Finally, the optimization process was determined using the softer cell-based smoothed FEM (as a branch of smoothed FEMs) results in comparison with standard FEMs results. These results show that the topology optimization design using the cell-based smoothed FEM ($nSD=4$), with 70% piezoelectric volume (weight) fraction, is preferred. So that, the optimum velocity obtained using this method is about 47% and 18% greater than the results of initial design and Q4-FEM analysis respectively. In spite of increasing velocity acquired through this algorithm, the final weight of this mechanism will be decreased about 14% respect to original motor.

The considered micromotor is currently being produced commercially, and it can substantially improve the efficiency of these piezoelectric micromotors.

Considering the possible reliability constraints during development of the optimum design of MEMS structures is recommended; most are due to inherent variations incurred during the manufacturing process.



(a)



(b)



(c)





(d)



(e)

Fig. 9 Our topology optimization designs with 70% volume fraction for : (a) Q4-FEM, (b) T3-FEM, (c) CS-FEM ($nSD=2$), (d) CS-FEM ($nSD=4$), and (e) CS-FEM ($nSD=8$)

Table 3 Comparison of our topology optimization design with initial one

Type of Design	Micromotor Approximate Weight(gr)	Micromotor Velocity (mms^{-1})	Microbeam Configuration (for design domain)
Initial Design	320	0.594	
Final Optimum Design	275	0.962	

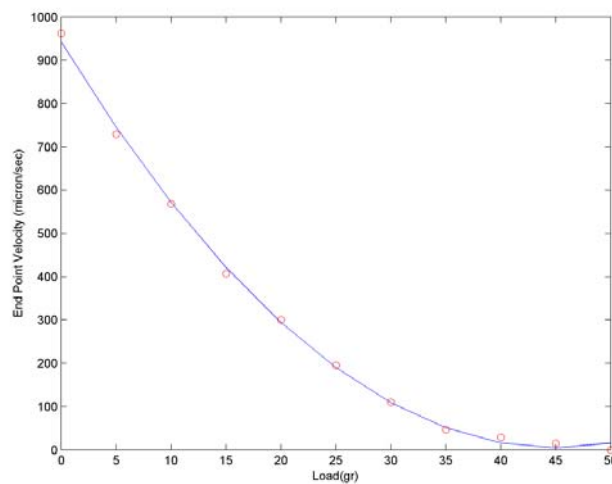


Fig. 10 Optimal end point velocity of each microbeam via applied external load

References

- Allik, H. and Hughes, T.J.R. (1970), "Finite element method for piezo-electric vibration", *Int. J. Numer. Meth. Eng.*, **2**(2), 151-157.
- Arora, J.S. (2004), *Introduction to optimum design*. 2nd edition, Elsevier academic press.
- Begg, D.W. and Liu. X. (2000), "On simultaneous optimization of smart structures- Part II: algorithms and examples", *Comput. Method. Appl. M.*, **184**(1), 25-37.
- Bendsoe, M.P. (1989), "Optimal shape design as a material distribution problem", *Struct. Optimization*, **1**(4), 193-202.
- Bendsoe, M.P. and Kikuchi, N. (1988), "Generating optimal topologies in structural design using a homogenization method", *Comput. Method. Appl. M.*, **71**(2), 197-224.
- Bendsoe, M.P. and Sigmund, O. (1999), "Material interpolations in topology optimization", *Arch. Appl. Mech.*, **69**(9-10), 635-654.

- Bendsoe, M.P. and Sigmund, O. (2003), *Topology optimization: theory, methods and applications*, Springer, Berlin.
- Benjeddou, A. (2000), "Advances in piezoelectric finite element modeling of adaptive structural elements: a survey", *Comput. Struct.*, **76**(1-3), 347-363.
- Bordas, S.P.A., Rabczuk, T., Hung, N.X., Nguyen, V.P., Natarajan, S., Bog, T., Quan, D.M. and Hiep, N.V. (2010), "Strain smoothing in FEM and XFEM", *Comput. Struct.*, **88**(23-24), 1419-1443.
- Carbonari, R.C., Nader, G. and Silva, E.C.N. (2006), "Experimental and numerical characterization of piezoelectric mechanisms designed using topology optimization", *Int. ABCM symposium series in Mechatronics*, **2**, 425-432.
- Carbonari, R.C., Silva, E.C.N. and Nishiwaki, S. (2005), "Design of piezoelectric multi-actuated microtools using topology optimization", *Smart Mater. Struct.*, **14**(6), 1431-1447.
- Chang, S.J., Rogacheva, N.N. and Chou, C.C. (1995), "Analysis of methods for determining electromechanical coupling coefficients of piezoelectric elements", *IEEE T. Ultrason. Ferr.*, **42**(4), 630-640.
- Chen, J.S., Wu, C.T. and Yoon, S. Y. (2001), "A stabilized conforming nodal integration for Galerkin mesh-free methods", *Int. J. Numer. Meth. Eng.*, **50**, 435-466.
- Choi, K.K. and Kim, N.H. (2005), *Structural sensitivity analysis and optimization*, Springer Science and Business Media, Inc., New York.
- Dai, K.Y., Liu, G.R. and Nguyen, T.T. (2007), "An n-sided polygonal smoothed finite element method (nSFEM), for solid mechanics", *Finite Elem. Anal. Des.*, **43**(11-12), 847-860.
- Donoso, A.; Sigmund, O. (2009), "Optimization of piezoelectric bimorph actuators with active damping for static and dynamic loads", *Struct. Multidiscip. O.*, **38**(2), 171-183.
- Friend, J., Umeshima, A., Ishii, T., Nakamura, K. and Ueha, S. (2004), "A piezoelectric linear actuator formed from a multitude of bimorphs", *Sensor. Actuat. A- Phys.*, **109**(3), 242-251.
- Huang, X. and Xie, Y.M. (2010), *Evolutionary Topology Optimization of Continuum Structures Methods and Applications*, John Wiley and Sons Ltd.
- Jensen, J.S. (2009), *A Note on Sensitivity Analysis of Linear Dynamic Systems with Harmonic Excitation, Report*. Department of Mechanical Engineering, Technical University of Denmark.
- Kang, Zh. and Wang, X. (2010), "Topology optimization of bending actuators with multilayer piezoelectric Material", *Smart Mater. Struct.*, **19**, 075018(11p).
- Kim, J.E., Kim, D.S., Ma, P.S. and Kim, Y.Y. (2010), "Multi-physics interpolation for the topology optimization of piezoelectric systems", *Comput. Method. Appl. M.*, **199**(49-52), 3153-3168.
- Kogl, M. and Silva, E.C.N. (2005), "Topology optimization of smart structures: design of piezoelectric plate and shell actuators", *Smart Mater. Struct.*, **14**(2), 387-399.
- Liu, G.R., Dai, K.Y., Lim, K.M. and Gu, Y.T. (2003), "A radial point interpolation method for simulation of two-dimensional piezoelectric structures", *Smart Mater. Struct.*, **12**(2), 171-180.
- Liu, G.R., Dai, K.Y. and Nguyen, T.T. (2007), "A smoothed finite element method for mechanics problems", *Comput. Mech.*, **39**(6), 859-877.
- Liu, G.R. and Nguyen, T.T. (2010), *Smoothed finite element methods*, CRC press, Taylor and Francis group.
- Liu, G.R., Nguyen, T.T., Dai, K.Y. and Lam, K.Y. (2007), "Theoretical aspects of the smoothed finite element method (SFEM)", *Int. J. Numer. Meth. Eng.*, **71**(8), 902-930.
- Liu, G.R., Nguyen, T.T. and Lam, K.Y. (2009), "An edge-based smoothed finite element method (ES-FEM) for static, free and forced vibration analyses of solids", *J. Sound Vib.*, **320**(4-5), 1100-1130.
- Liu, G.R., Nguyen, X.H. and Nguyen, T.T. (2010), "A theoretical study on the smoothed FEM (S-FEM) models: Properties, accuracy and convergence rates", *Int. J. Numer. Meth. Eng.*, **84**(10), 1222-1256.
- Long, C.S., Loveday, P.W. and Groenwold, A.A. (2006), "Planar four node piezoelectric with drilling degrees of freedom", *Int. J. Numer. Meth. Eng.*, **65**(11), 1802-1830.
- Nguyen, X.H., Liu, G.R., Nguyen, T.T. and Nguyen, C.T. (2009), "An edge-based smoothed finite element method for analysis of two-dimensional piezoelectric structures", *Smart Mater. Struct.*, **18**(6), 065015(12pp).

- Ohs, R.R. and Aluru, N.R. (2001), "Meshless analysis of piezoelectric devices", *Comput. Mech.*, **27**(1), 23-36.
- Rozvany, G., Zhou, M. and Birker, T. (1992), "Generalized shape optimization without homogenization", *Struct. Optimization*, **4**(3-4), 250-254.
- Sadeghbeigi Olyaie, M., Razfar, M.R. and Kansa, E.J. (2011), "Reliability based topology optimization of a linear piezoelectric micromotor using the cell- based smoothed finite element method", *CMES*, **75**(1), 43-88.
- Sigmund, O. (1994), *Design of Material Structures Using Topology Optimization*, Ph.D. Thesis, Department of Solid mechanics, Technical University of Denmark.
- Sigmund, O. (1997), "On the design of compliant mechanisms using topology optimization", *Mech. Struct. Mach.*, **25**(4), 495-526.
- Silva, E.C.N. (2003), "Topology optimization applied to the design of linear piezoelectric motors", *Smart Mater. Struct.*, **14**(4), 309-322.
- Silva, R.C.N. and Kikuchi, N. (1999), "Design of piezocomposite materials and piezoelectric transducers using topology optimization- part III", *Arch. Comput. Method E.*, **6**(4), 305-329.
- Svanberg, K. (1987), "Method of moving asymptotes-a new method for structural optimization", *Int. J. Numer. Meth. Eng.*, **24**(2), 359-373.
- Sze, K.Y., Yang, X.M. and Yao, L.Q. (2004), "Stabilized plane and axisymmetric piezoelectric finite element models", *Finite Elem. Anal. Des.* **40**(9-10), 1105-1122.
- Ueha, S. and Tomikawa, Y. (1993), *Ultrasonic Motors-Theory and Applications*. Monographs in Electrical and Electronic Engineering, **29**, Clarendon Press, Oxford.